Results from the E835 Cylindrical Scintillating-Fiber Tracker

M. Ambrogiani, W. Baldini, D. Bettoni, R. Calabrese,
E. Luppi, R. Mussa and G. Stancari

Dipartimento di Fisica, Università di Ferrara, 44100 Ferrara (FE), Italy
Istituto Nazionale di Fisica Nucleare, Sezione di Ferrara, 44100 Ferrara (FE), Italy

Abstract. A cylindrical 860-channel scintillating-fiber tracker for the measurement of the polar coordinate θ has been built for experiment 835 at Fermi National Accelerator Laboratory; it was used during the data-taking period, from October 1996 through September 1997.

The high granularity, flexibility and fast response of the scintillating fibers are combined with the high quantum efficiency of the Visible-Light Photon Counters. From this combination, a new kind of detector arises, capable of high-resolution tracking, fast first-level kinematical triggering and single/double-track discrimination.

Results of the tracker performance are presented.

INTRODUCTION

As often happens in high-energy physics, a detector needed to be developed to extract rare reactions from a huge background. A constraint usually exists on the amount and rate of data that an acquisition system can manage. Also, fast high-luminosity data-taking is sought, but it requires radiation-hard detectors [1]. For its physics goals, the E835 collaboration decided to build a scintillating-fiber tracker (SFT) read out by Visible-Light Photon Counters (VLPCs).

The thinness of the fibers allows a precise position determination; their flexibility makes possible a high-precision measurement of the angle θ relative to the beam axis. Due to its fast response, a detector made of scintillating fibers can also be used in a first-level trigger logic. The VLPCs compensate for the small amount of light produced by the thin fibers, because of their high quantum efficiency. The homogeneity of their response makes the analog readout of each channel useful for pulse-height analysis. Moreover, both the attenuation length of the fibers and the gain of the VLPCs have been shown to be nearly independent of the data-acquisition rate, at E835 luminosities ($\approx 2 \cdot 10^{31}$ cm$^{-2} \cdot$ s^{-1}) [2].

THE EXPERIMENT

Experiment 835 studies the direct formation of charmonium mesons in antiproton-proton annihilations ([3], [4], [5], [6]). By scanning an interval of center-of-momentum (CM) energy and counting the number of events that satisfy the charmonium-formation hypotheses, we obtain an excitation curve from which we infer masses, widths and decay branching fractions of these ($c\overline{c}$) states. About 150 pb^{-1} worth of data in the CM energy region between 2.9 GeV and 4.2 GeV were collected during the data-taking period, which lasted from October 1996 through September 1997.

The antiproton beam is stored and stochastically cooled in the Antiproton Accumulator, where it intersects a gaseous hydrogen jet-target, defining an interaction region of about $5 \times 5 \times 5$ mm^3. The detector is designed to select the final states of the charmonium mesons that include electrons, positrons or photons. It is symmetrical around the beam axis and covers the polar angle from 15° (downstream region) to 65° (upstream). Its main components are an inner tracking system, a threshold Cherenkov counter and a lead-glass electromagnetic calorimeter, as shown in fig. 1.

The signature for charmonium formation is given by an electron and a positron with invariant mass around 3.1 GeV/c^2, indicating the inclusive production of the

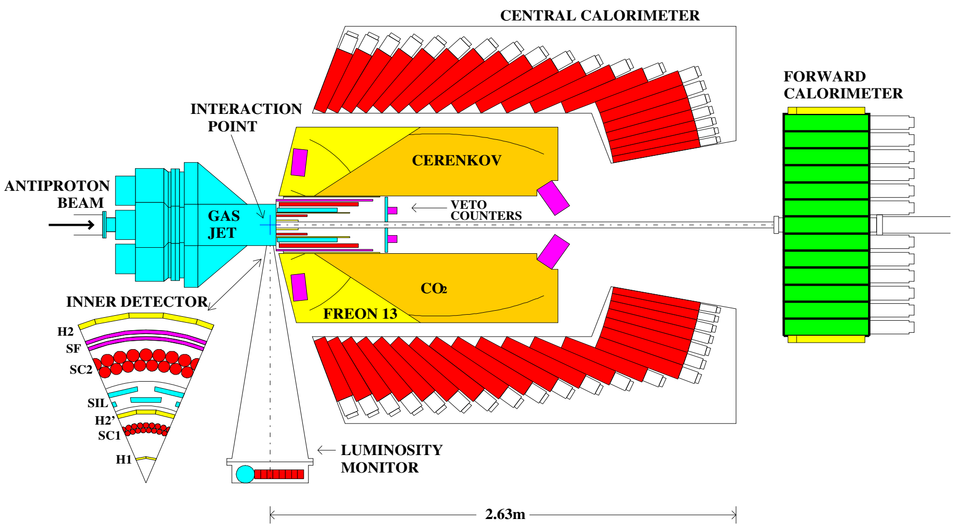

FIGURE 1. The E835 Detector. The inner tracking system consists of three hodoscopes (H1, H2', H2), two sets of straw tubes (SC1, SC2), silicon strips (SIL) and the two layers of scintillating fibers (SF). The central calorimeter is segmented in both θ (20 elements, shown) and ϕ (64 elements, not visible in the picture). The z axis of the lab frame (centered on the interaction point) is defined by the antiproton momentum, while y is the vertical axis.

J/ψ meson and its decay into an e^+e^- pair. Also, the decay of a charmonium state into two photons is directly detectable.

A complementary approach to the identification of charmonium uses hadronic final states. For the study of the $\eta_c(1^1S_0)$ state and the search for the $\eta_c'(2^1S_0)$ state, the processes $\bar{p}p \rightarrow \bar{p}p$ and $\bar{p}p \rightarrow \phi\phi \rightarrow K^+K^-K^+K^-$ were chosen. In this context, the SFT represented the ideal choice: high tracking resolution for the topological identification of those reactions and fast first-level trigger capabilities to improve the trigger performance.

THE SCINTILLATING-FIBER TRACKER

Detector Design

This cylindrical detector is used to measure the polar coordinate θ in the region between 15° and 65°. The 860 fibers are laid on two staggered layers. Following is a brief description of the layout of the tracker and of its readout. Details regarding the fibers (Kuraray SCSF-3HF-1500), the cylindrical supports, the VLPCs (HISTE-V, EOC-low), the cryostat and the readout electronics can be found in [2], [7] and [8].

LIGHT COLLECTION. Each scintillating fiber (core diameter = 740 μm) is wound around one of the two support cylinders (radii 144.0 mm and 150.6 mm), on the surface of which a set of U-shaped grooves has been machined (pitches 1.10 mm and 1.15 mm). The depth of the grooves varies linearly with the azimuthal coordinate ϕ,

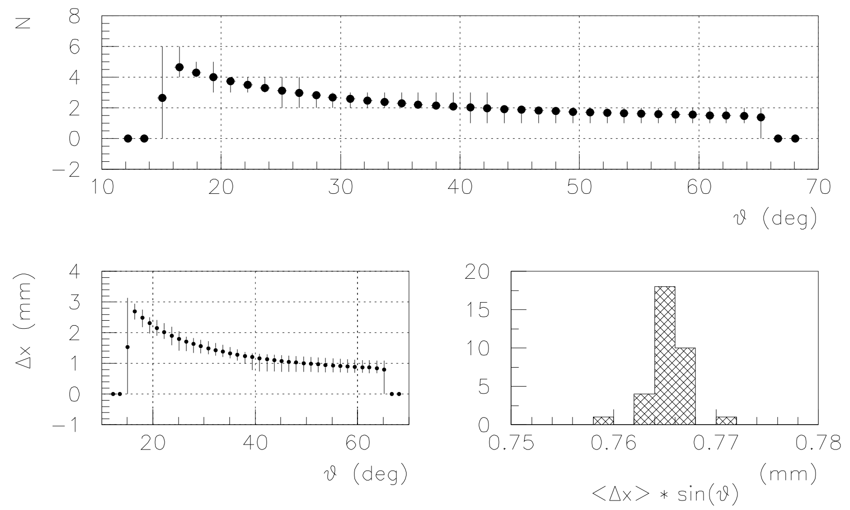

FIGURE 2. SFT design parameters from Monte Carlo calculations. The number N of hit fibers and the active thickness Δx of the detector are shown as a function of the polar angle θ. The dots represent the average over an arbitrary θ slice, while the error bars indicate the minimum and maximum possible values. The distribution of the average active thickness, multiplied by $\sin(\theta)$, is also plotted (lower right).

so that the fiber overlaps itself after one turn. On one end, the fibers are aluminized, to increase the light yield and improve its homogeneity; on the other end, they are thermally spliced to clear fibers, which, after a four-meter path, bring the light to the surface of the VLPCs, housed in a cryostat and kept at a temperature of 6.5 K.

Signal Readout. The electronic signal generated by the VLPCs is amplified by QPA02 cards, designed at Fermilab. After the amplification stage, the signal is sent to discriminator-OR-splitter modules, custom made in Ferrara. These modules provide an analog and a digital output for each input channel, together with the digital OR of all inputs. The analog signal is then sent to ADCs, while the digital output is read out by latches. The digital OR of a set ('bundle') of adjacent channels is sent to TDCs and to the first-level trigger logic of the experiment.

Geometrical Monte Carlo. Fig. 2 shows the number N of fibers (summed over both layers) whose core is intersected by a straight track originating from the interaction vertex; in order to maximize its geometrical acceptance, the detector has been designed so that, in the region $15° < \theta < 65°$, there is always at least one fiber on the track path. The active thickness Δx is the sum, over all hit fibers, of the track path lengths inside the traversed fiber cores; even though its fluctuations are not negligible, its mean $\langle \Delta x \rangle$ is proportional to $1/\sin(\theta)$; this yields to an extrapolated normal-incidence active thickness of 0.765 ± 0.001 mm.

The total thickness of the tracker, dominated by the acrylic support cylinders, corresponds to $\approx 10^{-2}$ radiation lengths per layer at normal incidence.

Detector Performance

Reliability of the Equipment. Throughout the run, the cryostat worked very efficiently. The liquid helium flux was constant and the temperature stable (6.500 ± 0.004 K). Four inevitable warm-ups occurred, due to scheduled shutdowns or to power outages; the temperature of the cryostat rose typically up to ≈ 70 K in a few hours. That was the main cause of loss of channels, attributed to the poor

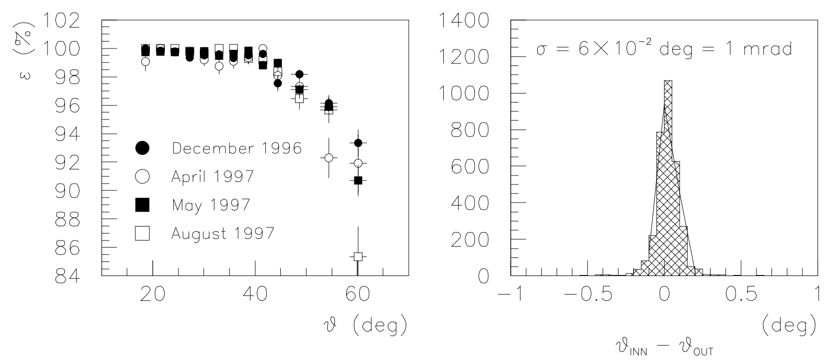

FIGURE 3. Tracking performance. On the right, the detection efficiency as a function of the polar angle and time; on the left, the distribution of θ residuals.

quality of the micro-welding joining the VLPC substrates to the electrical cables. Four channels out of 860 were not working at the beginning of the run; at the end, we had almost eighty dead channels [2].

SIGNAL. The pulse generated by a track crossing one fiber, as seen at the input of the discriminator-OR-splitter modules, is typically 180 mV high and 80 ns wide, corresponding to a collected charge ≈ 0.2 nC. The discriminator thresholds are set to about 40 mV.

DETECTION EFFICIENCY AND TRACKING RESOLUTION. We measured the detection efficiency with J/ψ-inclusive and ψ' events, when the J/ψ or ψ' decay into an e^+e^- pair ($\approx 4 \cdot 10^4$ events over the whole data-taking). For each track, we look for an associated hit in the SFT above a given software threshold (typically, 0.2 mip), within a polar window of ± 50 mrad; the results are shown in fig. 3. The seeming detection inefficiency at $\theta > 40°$ is actually accounted for by a loss of geometrical acceptance, caused by an improper mechanical alignment of the two layers (the relative shift, measured independently in two-body reactions, is 0.8 mm larger than the design value). Variations of the efficiency over time are due to different run conditions (gate width of the ADCs) and to loss of channels.

The SFT is by far the detector with the best spatial resolution in our apparatus. For this reason, we can only measure what we call 'intrinsic' tracking resolution, i. e. the standard deviation (divided by $\sqrt{2}$) of the distribution of the differences $\theta_{INN} - \theta_{OUT}$, where, for a given track, θ_{INN} (θ_{OUT}) is the polar angle measured by the inner (outer) layer. The resolution, averaged over all polar angles, comes out to be (0.7 ± 0.1) mrad, as shown in fig. 3.

SINGLE-FIBER AND DETECTOR CALIBRATION. In order to get, for each VLPC channel, the one-photoelectron (phe) equivalent in ADC counts (1 ADC count = 0.25 pC), we performed an LED test on all channels with the setup actually used

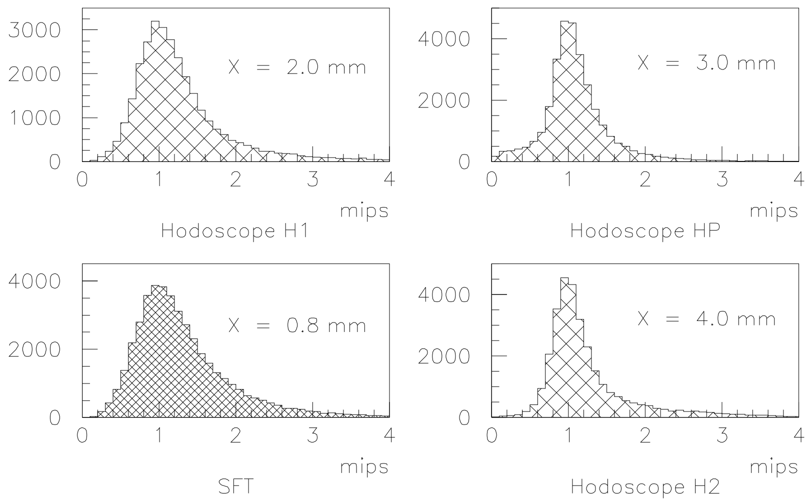

FIGURE 4. Comparison between the energy deposit distribution in three hodoscopes and in the SFT. X is the normal-incidence thickness.

in the experiment (VLPC cassettes, cryostat and readout electronics). The pulse charge in ADC counts generated by a minimum-ionizing particle, instead, is obtained studying a high-statistics hadronic sample of punch-through tracks in the electromagnetic calorimeter ($\approx 10^3$ events/fiber). The ADC/mip variable reflects fluctuations from many sources: the response of the scintillating fibers; the light transmission of the connections; the coupling between clear fibers and VLPC surfaces; the gains of the VLPCs and of the amplifiers; and the readout electronics. Still, the distribution of this variable shows an excellent homogeneity (mean $\approx$ 400 ADC/mip, standard deviation $\approx$ 12%). The mean number of photoelectrons per minimum-ionizing particle turns out to be distributed around 14 phe/mip. More details can be found in [2], [8] and [7].

PULSE-HEIGHT ANALYSIS AND SINGLE/DOUBLE-TRACK DISCRIMINATION. Fig. 4 shows a comparison between the fluctuations of the energy deposit in the scintillating-fiber tracker and those in a traditional hodoscope/phototube system. The normal-incidence thicknesses X are very different (≥ 2 mm for the hodoscopes, < 0.8 mm for the SFT) and so are the light-guide lengths L (typically 50–100 cm between a hodoscope and a phototube, while the clear fibers are more than four meters long); also, the thickness oscillations of the SFT are significant. Still, the fluctuations of the energy deposit in the SFT (hence the amount of light collected) are comparable with those in hodoscope H1.

These relatively small fluctuations, together with the good spatial resolution, can be helpful when applied to suppress a kind of background particularly important for E835, and common to many high-energy-physics experiments: e^+e^- pairs with small opening angle, generated by photon conversions or by Dalitz decays of neutral pions, simulating a single track.

The tools that we use off-line to reject this background are the pulse height in

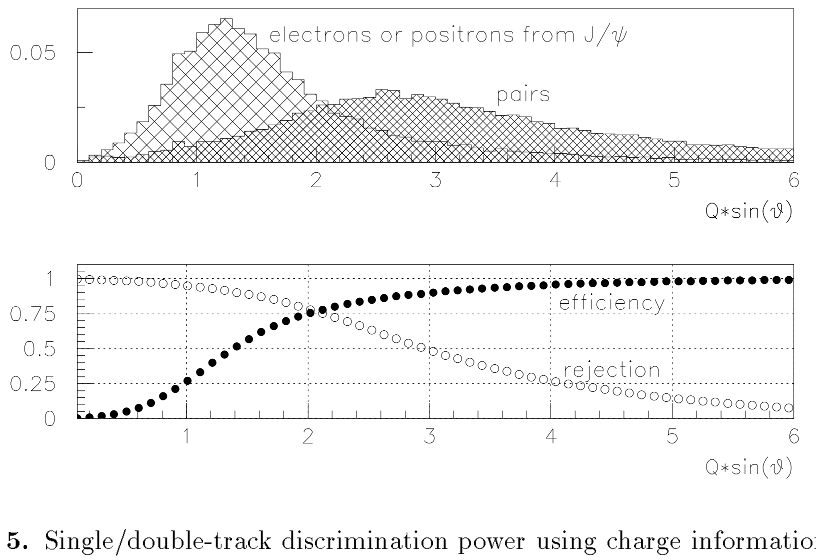

FIGURE 5. Single/double-track discrimination power using charge information only. A clean sample of electrons or positrons is compared with a sample of pairs.

the hodoscopes, the signal in the threshold Cherenkov counter and the energy and shape of the showers in the central calorimeter. The SFT can add two tools: pulse height and granularity. When the opening angle of the e^+e^- pair is so small that just one cluster (defined as a set of adjacent hit fibers) is generated, the energy deposit is likely to be big; whereas when the pair's separation is big enough, an extra cluster in the detector will appear. In fig. 5 one can see the discrimination, based on charge deposition only, between a clean sample of single tracks (electrons or positrons) and a sample of pairs, defined as charged tracks which, combined with a neutral deposit in the central calorimeter, form a π^0 invariant mass. Q is the sum of the charges deposited in all SFT clusters in a $\pm 2°$ window centered around the track. For instance, a 50% rejection factor is achieved with 90% efficiency, cutting at $Q \cdot \sin(\theta) = 3$.

Timing Resolution. In order to evaluate the intrinsic time resolution of the detector, we select those tracks that hit at least two fibers belonging to adjacent bundles, and are therefore read out by different TDC channels. We then define the time resolution as the standard deviation, divided by $\sqrt{2}$, of the distribution of the variable $t_i - t_{i+1}$, when the same track crosses both a fiber of bundle i and a fiber of bundle $i+1$ ($i = 1, 18$). This intrinsic time resolution comes out to be around 3.5 ns, as can be seen in fig. 6; it is mostly due to the decay time of the scintillator.

First-Level Trigger. Given the excellent timing performance of the detector in terms of both fast response and intrinsic resolution, a fast first-level trigger logic based on the SFT was designed. The goal is to observe the decay of the $\eta_c(1^1S_0)$ and $\eta_c'(2^1S_0)$ mesons into $\phi\phi \to K^+K^-K^+K^-$ and the interference between resonant and elastic $\bar{p}p$ final states near 90° in the CM frame. Coincidences between sets of fiber bundles can select the right polar kinematics, whereas the hodoscopes provide azimuthal information. This first-level selection yields affordable trigger rates — 20–110 Hz for the $\bar{p}p$ trigger and 600–1000 Hz for the $\phi\phi$ trigger, as the CM energy varies between 4.2 GeV and 2.9 GeV.

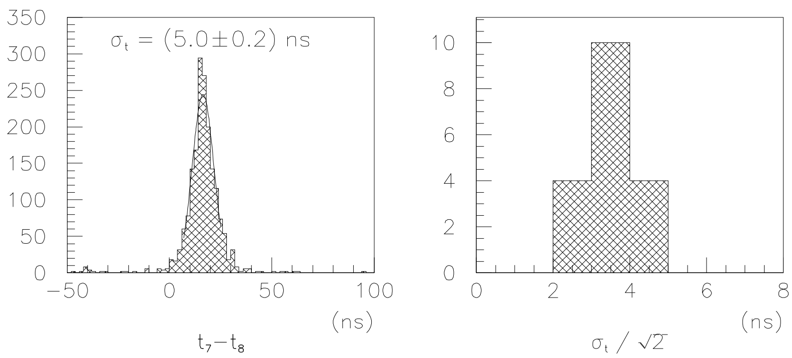

FIGURE 6. Intrinsic time resolution. The first plot shows the time difference distribution for a couple of adjacent bundles, while the one on the right is the standard-deviation distribution for all eighteen couples of adjacent bundles.

CONCLUSIONS

We presented the results of the first detector used in a high-energy-physics experiment which exploits scintillating fibers and Visible-Light Photon Counters.

It is a unique detector, because it combines a high tracking performance (resolution < 1 mrad, detection efficiency $\approx 99.5\%$), fast first-level trigger characteristics (time spread < 5 ns) and single/double-track discrimination power.

The technique is ready for future large-scale applications.

ACKNOWLEDGEMENTS

The realization of this project would not have been possible without the valuable support of the Fermilab Particle Physics Division; the Fermilab Cryogenics Group; the D0 and CDF Collaborations at Fermilab; the University of Ferrara and INFN; and, of course, the E835 collaborators. In particular, we wish to thank Alan Bross (Fermilab and D0 Collaboration) and Stephen Pordes (Fermilab, Particle Physics Division).

Discussions with M. Atac, C. Lindenmeyer, M. Mishina and R. Richards represented a source of helpful suggestions and effective ideas.

REFERENCES

1. Ruchti R. C., *Ann. Rev. Nucl. Sci.* **46**, 281–319 (1996).
2. Mussa R., "Performance Measurements on Histe-V VLPC Photon Detectors for E835 at FNAL", in these proceedings.
3. Pastrone N. (for the E835 Collaboration), "New Results from E835 at Fermilab Antiproton Accumulator — Study of ($c\bar{c}$) States formed in Antiproton-Proton Annihilations", presented at the 4th International Workshop on Progress in Heavy-Quark Physics, Rostock, Germany, September 20–22, 1997.
4. Zioulas G. (for the E835 Collaboration), "First Results on Charmonium Spectroscopy from Fermilab E835", presented at the 7th International Conference on Hadron Spectroscopy, Brookhaven National Laboratory, Upton, New York, August 25–30, 1997.
5. Cester R. and Rapidis P. A., *Ann. Rev. Nucl. Sci.* **44**, 329–371 (1994).
6. Armstrong T. et al. (E760 Collaboration), Fermilab Proposal P-835-REV (1992).
7. Luppi E., "The E835 Scintillating-Fiber Tracking Detector", presented at the 5th International Conference on Advanced Technologies and Particle Physics, Villa Olmo (CO), Italy, October 1996.
8. Ambrogiani M. et al., *IEEE Trans. Nucl. Sci.* **44**, 460–463 (1997).